THE DESIGN, DEVELOPMENT AND CONSTRUCTION OF A LOW-NOISE, LOW-TURBULENCE WIND TUNNEL

by
Carl E. Hanson
B.S., University of Minnesota
(1965)

SUBMITTED IN PARTIAL FULFILLMENT
OF THE REQUIREMENTS FOR THE
DEGREE OF MASTER OF
SCIENCE
at the
MASSACHUSETTS INSTITUTE OF
TECHNOLOGY
January, 1967

Signature of Author ...Carl E. Hanson.....
Department of Mechanical Engineering, January 16, 1967

Certified by .....Patrick Leehey.....
Thesis Supervisor

Accepted by .....
Chairman, Departmental Committee on Graduate Students

The Design, Development and Construction of a Low-Noise, Low-Turbulence Wind Tunnel

by
Carl E. Hanson

Submitted to the Department of Mechanical Engineering on January 16, 1967 in partial fulfillment of the requirement for the degree of Master of Science in Mechanical Engineering.

ABSTRACT

A low-noise, low-turbulence, subsonic wind tunnel was designed for investigating both wide and narrow band flow noise processes. The open-circuit design incorporates such innovations as interchangeable open jet and closed duct test sections within a sealed test chamber which can be either reverberant or anechoic by the use of removable wall treatment. Low noise level at the test section is achieved by using upstream treatments such as a honeycomb of soda straws and an exterior fiberglass covering on the contraction, and by using downstream treatments such as a combination muffler-diffuser and another honeycomb of soda straws. Low turbulence level is achieved by using the honeycomb, damping screens, and a large area contraction ratio.

Final measurements of the aerodynamic performance verify the preliminary estimations of tunnel drag losses and power requirements. Moreover, results show that the original design criteria are met successfully.

Thesis Supervisor: Patrick Leehey
Title: Associate Professor, Naval Architecture and Mechanical Engineering

ACKNOWLEDGEMENTS

The author wishes to express his thanks and appreciation to Professor Patrick Leehey for his many suggestions and contributions which were vital to the development of this project. Appreciation is extended to Ray Carter of F. W. Dixon Company for his suggestions on construction details. Thanks are also due to Signe Anderson, Larry Wittig, Leonard Kurzweil, Sanford Kornfeld, and Curtis Marx for their assistance and encouragement.

TABLE OF CONTENTS

FIGURES

I. Introduction

The subject of generation of hydrodynamic and aerodynamic noise has received a great deal of attention lately, largely due to problems arising from jet noise and boundary layer noise. Theories have been developed providing the basis for the understanding of the laws governing the generation of aerodynamic sound [1]. However, direct experimental confirmation of the theories has not been accomplished, mainly due to the lack of the necessary facilities.

Moreover, much of the work that has been done with boundary layer noise, such as the measurement of wall pressure fluctuations, has been limited by the noise levels in the various wind tunnels in which the measurements were carried out.

A program of research in the area of flow noise has been instituted in the Acoustics and Vibrations Laboratory at Massachusetts Institute of Technology. The type of tests anticipated include investigations of both narrow band and wide band flow noise processes such as Aeolian tones, boundary layer excited panel vibrations, and wall pressure fluctuations. The first necessary step in this program was the construction of an air duct facility meeting low noise and low turbulence requirements.

The preliminary design points for this facility include:

(a) A uniformly distributed maximum mean velocity of

180 ft/sec in a 15 inch square test section,

(b) Either open jet or closed duct test section capability,

(c) A turbulence level of 0.1 % in the uniform mean velocity area at the test section,

(d) A background noise level in the test chamber 10 db below signal level for each type of test with the low frequency cutoff at 200 cps.

The open circuit wind tunnel layout lends itself to treatment in three separate sections: an upstream section, a test section, and a downstream section (Figure 1). The details of the design concepts for each section are discussed in this report.

II. Design Criteria

A. Upstream Section

The upstream section consists of an inlet, a honeycomb, screens, and a contraction (Figure 2). Design of this section was influenced by three criteria: low-noise, low-turbulence, and a uniform velocity profile. A criterion of secondary importance, but still significant, was minimal drag loss to achieve the highest possible velocity in the test section.

A-1. Inlet

The inlet provides a direct opening to the honeycomb section. The cross-section is a square 67 inches on a side.

Since the laboratory space provides the return loop of the open-circuit wind tunnel, the location of the inlet away from obstructions is of primary importance. A minimum of 5 feet clearance to the nearest wall and 1 1/2 feet clearance to the floor is allowed. To ensure a smooth entry of the return around the edges of the inlet, an 8-inch diameter round collar is attached at the periphery.

A-2. Honeycomb

A honeycomb is generally utilized only as a flow-straightening device. It aids in breaking up large-scale eddies and swirls which may be present at the inlet. However, there is some evidence to the effect that a wall of small

tubes such as soda straws serves to attenuate the transmission of a diffuse sound field [2]. Preliminary tests tended to confirm this evidence for the attenuation of frequencies above 4000 cps. Thus, in addition to its use as a flow-straightener, a honeycomb of this sort can be used to diminish noise transmitted through the inlet.

Accordingly, the honeycomb is constructed of approximately 130,000 plastic soda straws, 3/16 inches in diameter and 10 1/2 inches in length, carefully stacked in a hexagonal close-packed configuration and held in place fore and aft by 18-mesh screening (Figure 3). The choice of plastic straws over paper is dictated by durability considerations and by the fact that the extrusion process results in seamless construction and clean-cut ends. The whole section proved to be quite inexpensive and relatively easy to construct.

A-3. Screens

Low-turbulence levels at the test section requires the use of fine mesh screens in the low velocity settling chamber before the contraction. Such screens remove large-scale eddies and introduce a great number of small eddies which decay rapidly [3], [4]. However, the Reynolds number based on wire diameter must be less than about 60 if the screens are not to add turbulence of their own [5]. Moreover, imperfections in screens have been reported to produce

slowly decaying longitudinal fluctuations [4].

A section of four 18 mesh screens with wire diameter of 0.010 inches is used in the tunnel. The Reynolds number based on wire diameter is 40 to satisfy the no self-turbulence criterion. Further, each screen was cut from a 7 foot wide roll to avoid a seam imperfection. Special care was exercised in handling and stretching the screens, each being mounted on a readily removable frame in case the need for replacement arises.

A rough estimate of the effect in reducing turbulence can be made by using the turbulence reduction factor

$$f = (1 + k)^{-n/2}$$

where k = screen pressure-drop coefficient, and n = number of screens. With four 18 mesh screens in place, the turbulence reduction factor becomes of the order of 0.10. This factor cannot be used in estimating the turbulence level in the test section as we have no reliable estimate of the turbulence level at the inlet. However, a turbulence reduction factor of 0.10 does give indication that screens are indeed necessary to achieve low-turbulence at the test section.

A-4. Contraction

The contraction section was designed with velocity requirements and size limitations in mind. From reports on the effect of contraction cones in decreasing velocity

variations in the flow [6, p. 67] and in reducing the longitudinal turbulence component [4], it appeared desirable to use the largest feasible area contraction ratio. Considerations of laboratory space limitations and test section size determined an area contraction ratio of 20:1 over a length of 5 to 6 feet.

The actual shape of the contraction section for a short length is not easily determined. Care must be exercised so that separation does not occur along the walls or this could lead to extreme fluctuations at the test section. Theoretical approaches have been limited to potential flow considerations [7], [8] and as such are not directly applicable to this case. Maestrello reported having success with a contraction with the curve of a ninth degree polynomial [9]. The advantage of this approach is that the transition from settling chamber to contraction and from the contraction to the test section can be varied merely by specifying derivatives.

Two ninth degree polynomial curves were drawn which gave our 20:1 area contraction. In the first curve, the contraction length was limited to 5 feet. The function and its first five derivatives were set equal to zero at the exit and the first three derivatives were set equal to zero at the inlet. These, along with the contraction ratio served to specify each of the ten constants obtaining the equation:

$$y = 26.05\ \xi^6 (-56\ \xi^3 + 189\ \xi^2 - 216\ \xi + 84) \quad \text{where } \xi = \frac{x}{60} .$$

The shape is shown as the heavy line in Figure 11b. A second curve was then developed with the same contraction ratio over a length of 6 feet. This curve was determined by setting the function and its first six derivatives equal to zero at the exit and by setting the first two derivatives equal to zero at the inlet. This results in the equation:

$$y = 26.05 \frac{\xi^7}{6^7} \left(\frac{7}{9} \xi^2 - \frac{21}{2} \xi + 36\right) \quad \text{where} \quad \xi = \frac{x}{12} ,$$

which has the shape shown as the heavy line in Figure 11a. This curve has a much more gradual transition to the test section than the previous curve at the expense of a steeper initial slope at the inlet. However, since the exit velocity is much higher than the inlet velocity, a smoother transition is necessary to prevent separation.

Scale model contraction sections using each of the above curves were then constructed of fiberglass with static pressure taps at various stations along the walls. Tests were conducted on these models in a small low-turbulence open jet wind tunnel. The results (Figure 11) show the static pressure distribution along the wall of each contraction. The static pressure at each of taps #1 reflects a small loss from the upstream static pressure. However, after remaining almost constant through most of the area reduction, it drops rapidly to a negative value. This is as expected from the equations of motion in streamline coordinates. However, the static wall pressure of contraction #1 (Figure 11b) dropped more quickly

to a lower value at the exit than did the pressure for contraction #2 (Figure 11a). This is an indication that the velocity increase at the wall of contraction #2 is also more gradual, thus making separation less likely. Moreover, the higher static pressure at the exit of contraction #2 indicates there is less drag loss in this section. The conclusion drawn from this testing program was that contraction #2 was certainly the better choice.

The full size contraction section follows the curve of contraction #2. It is constructed as a wooden frame overlaid with 1/8 inch bending plywood. Sufficient framework reinforcement is necessary to hold the shape at all points, but especially in the high velocity section where the underpressure is about 0.2 psi. The section has an exterior covering of fiberglass with density 12 lb/ft^3 to minimize sound transmission to the interior.

The final specifications for the contraction are:

cross-section:	square, 67 inches on a side at inlet, 15 inches on a side at exit
area ratio:	20 to 1
length:	6 feet
curve:	defined by the equation $y = 26.05 \frac{\xi^7}{6^7} \left(\frac{7}{9}\xi^2 - \frac{21}{2}\xi + 36\right)$ where $\xi = \frac{x}{12}$ and x = length coordinate in inches with origin at the exit.

B. Test Section

The wind tunnel at the contraction exit penetrates a chamber which encloses either the closed duct or the open jet test section (Figure 4). In addition to being interchangeable, the test sections may be moved to various positions along the entire 13 feet, 6 inches of ducting within the chamber. This is of advantage in work requiring different boundary layer thicknesses.

B-1. Reverberant/Anechoic Chamber

Since this wind tunnel is to be used primarily for measurement of both narrow and wide band flow noise levels, it is necessary to have the appropriate test chamber for making these sound measurements. For diffuse field acoustic power measurements, a reverberation chamber is required, but for free field sound pressure level and directivity pattern measurements, an anechoic chamber is required. It is anticipated that all of the above measurements will at some time be required. Thus the test chamber has been designed with flexibility in mind in that both reverberant and anechoic modes are possible by merely changing the wall treatment.

The three primary criteria for the chamber design were as follows:

(1) The transmission loss of the walls, floor, and door must be sufficient to have the background noise in the test chamber 10 db below signal level for each type of test contemplated with fan operating at maximum capacity.

(2) The interior wall absorption coefficient must be sufficiently small and chamber size must be sufficiently large to permit acoustic power level measurements by reverberant chamber techniques to be made in 1/3 octave bands at least as low as the band centered on 200 cps.

(3) Anechoic treatment and chamber size must be sufficient to permit free field sound pressure level measurements to be made over a half space down to 200 cps.

For the first criterion, estimations were made of the fan noise from data by the various fan manufacturers. This along with the laboratory room characteristics gave an estimate of the noise level in the laboratory space. Several wall constructions were then considered and the transmission loss of each was estimated using published data [10]. Finally, predictions of the signal levels of each type of test contemplated were made from published similar tests. From this information the decision was made to use mortar-filled 6 inch cement block walls, a 5 inch poured concrete ceiling, and a 40 - 60 db transmission loss door.

The second criterion is satisfied by the choice of wall materials and the sizing of the chamber. Basic reverberation chamber requirements dictate a minimum of 20 room modes in the lowest 1/3 octave frequency band of interest and a non-integer relationship between any two of the room dimensions, length, height, and width [10, pp. 176-177].

The center frequency of 200 cps requires a room with volume of 850 ft^3. Preliminary calculations showed that a chamber length of 13 feet, 6 inches is adequate for measurements of power radiated from panels, allowing proper distancing of microphones from the walls. This fixed the room dimensions at 13 feet, 6 inches long, 9 feet wide and 7 feet high.

The third criterion could be met by the classical anechoic wedge treatment applied to wall, ceiling, and floor surfaces of the chamber. An inexpensive alternative, however, is to hang thick fiberglass blankets slightly away from the walls and ceiling. This treatment, of course, changes the description from "anechoic" to "semi-anechoic" since the low frequency cutoff is not as sharply defined as with the wedge installation. Either of the two installations are possible in the chamber.

Two aspects of anechoic chamber design are considered. First, the level of the diffuse sound field must be 10 db below the direct signal level from the source in order to avoid interference. Second, the level of the reflected signal very near the wall must be 10 db below the direct signal level from the source. These two criteria are satisfied in this chamber size by using the fiberglass blanket installation and by setting the low frequency cutoff at 200 cps.

The wall treatment selected consists of a 3 inch blanket of fiberglass spaced out 3 inches from the walls and

ceiling by mechanical fasteners. More specifically, the blanket consists of a 1.5 inch layer of 0.5 lb/ft^3 fiberglass and a 1.5 inch layer of 1.5 lb/ft^3 fiberglass separated by a flexible canvas septum. The fasteners penetrate the canvas septum and hold the blanket in place with washer-like holding plates. The floor is covered with a 2 inch thick fiberglass board of 12 lb/ft^3 density and a layer of the 3 inch wall treatment.

Great care is exercised to avoid sound shorts into the chamber from exterior electrical conduits, air leaks, and wind tunnel structure. Conduits are isolated by rubber sections and all penetrations of cables and power leads into the chamber are sealed. The two test section penetrations of the walls are sealed all around with a 1/4 inch layer of silicone rubber sealant. This also helps damp out any tunnel wall vibrations which enter the chamber.

B-2. Ducts and Test Sections

The ducting through the entire length of the chamber is 3/4 inch plywood, square cross-section of 15 inches on the interior side with a small fillet at the corners. It is made of three removable sections of different lengths to allow positioning of the test sections at various distances along the chamber length. The sections attach to each other by means of flanges at the ends, and, in addition, each is held in place by cables from the chamber ceiling and floor.

The cable supports are isolated from vibrations by rubber mountings.

The open jet test section (Figure 5) is obtained by installing a collector in the gap between two long duct sections. The collector has been designed so that its leading edge interior will run along the constant mass flux boundary of the jet. This design allows 10 inches of open jet flow.

The closed duct test section (Figure 6) is constructed to bridge the gap between the two long sections. Alignment is achieved with pins in the hardwood flanges. A plexiglass door allows ready access to probes, models, and plates which may be mounted in one of the other sides.

C. Downstream Section

The downstream section includes a muffler-diffuser, a honeycomb of soda strams, an adjustable-gap coupling between the diffuser and the centrifugal blower and the blower itself.

C-1. Muffler-Diffuser

In order to isolate blower-generated noise from the test section, a muffler is incorporated in the diffuser section. This muffler is basically a fiberglass filled box through which the expanding diffuser passes and a fiberglass cruciform wedge which is placed in the diffuser duct. The box is constructed of 0.75 inch plywood with appropriate reinforcing and is 8 feet long, 4 feet wide and 7.5 feet high.

It is filled around the flow duct with layers of 2 lb/ft^3 density fiberglass. The flow duct is 15 inch square cross section at the inlet and is circular with 40.25 inch diameter at the exit. Transition from square to round occurs along the entire length of the muffler. The surface of the duct is made up of fiberglass cloth and wire screen of very low flow resistance in order not to impair the absorption of sound by the fiberglass packing. Within the duct is an 8 foot fiberglass cruciform wedge to absorb the high frequencies (Figures 7 and 8). The wedge is constructed of dense 12 lb/ft^3 fiberglass on a masonite framework and is faced with layers of shear flow resistant fiberglass and fiberglass cloth.

In addition to its acting as a muffler, this section also serves as a diffuser for the flow, although of necessity it does not conform to good diffuser design practices. The main effect is the area increase which is the same as that for a 15° cone over the entire length of 8 feet. However, the first half of this length is only a slight increase in area due to the presence of the cruciform wedge, and the second half experiences an increase much more like that of a 23° cone. Neither of these angles approach the theoretical optimum of 5° to 7° [3, p. 56]. On the other hand, the rough walls will build up a thick boundary layer which will tend to minimize losses from separation.

C-2. Honeycomb of Soda Straws

A honeycomb of soda straws is employed between the muffler-diffuser and the blower to aid in attenuating high frequency sound. A secondary purpose is to reduce the fourth angular harmonic of the cruciform wake impinging on the 12 bladed centrifugal blower. This should help in reducing the blade frequency component of blower noise.

C-3. Adjustable-Gap Coupling

In order to avoid any surging problems with models of high blockage in the test section, a sliding ring is provided which couples the muffler section with the fan. The ring can be opened to relieve any unstable back pressures that may cause fluctuations at the test section. In addition, this gap provides vibration isolation between the blower and the rest of the tunnel.

C-4. Blower and Motor

The blower is a Chicago Blower size 36 1/2 single inlet, single discharge centrifugal type with a 39 3/8 inch wheel diameter (Figure 9). The inlet is circular with 40 5/8 inch diameter and the discharge is rectangular 35 5/8 inches by 32 inches. It is matched to the tunnel requirements with a rating point of 16,800 cfm against 5 inches static pressure at 960 rpm and 16 h.p. The 12 blades are backward-slanted airfoil shape which are reported to have lower noise rating than other types [11, 25: p. 3].

Octave band sound power level data from the manufacturer tended to confirm this.

Power is provided by a 20 h.p. shunt-wound DC motor with a continuously variable 4:1 speed range (Figure 10). Speed control is provided by a rheostat which varies the field current. The motor drives the fan by a V-belt pulley arrangement. An additional idler pulley is used for very low flow velocities.

Both motor and blower are mounted on a single vibration-isolation base (Figure 9). The base is designed to minimize the transmission of structural vibrations to the test chamber caused by the motor or the blower. Special effort was taken to reduce rocking and rotational modes of vibration by providing a near center of gravity mounting with resonant frequency just above the maximum motor and blower rotational frequencies. This gives us effective isolation well below the 200 cps low frequency cutoff criterion. Mounting isolation is achieved by commercially available ribbed neoprene rubber pads.

III. Estimation of Power Factor

Friction losses in the wind tunnel are reflected in loss of static pressure for each section. The product of this loss and the area over which it appears yields the drag of the section. And finally one obtains the power lost by multiplying the drag and the velocity. Rather than summing up the power lost for each section, it is customary to express the loss in terms of a loss coefficient:

$$K = \frac{\Delta p\ A}{\frac{1}{2}\rho A V^2} = \frac{\Delta p}{q} \quad \text{where} \quad q \equiv \frac{1}{2}\rho V^2 .$$

To circumvent having to compute q for each section, a new loss coefficient is defined which refers everything to the q at the test section [6, p. 69]:

$$K_o \equiv K\frac{q}{q_o} = \frac{\Delta p}{q_o} \quad \text{where} \quad q_o = \frac{1}{2}\rho V^2 \quad \text{at the test section.}$$

A summation of the coefficients of all sections yields the total static pressure drop which must be balanced by the static pressure rise through the fan.

In the loss estimations which follow, Pope's [6] notation is used throughout with the slight modification that area ratios are used to refer local velocities to the test section velocity.

A. Static Pressure Loss

A-1. Honeycomb

In this section we have stacked soda straws held in place by screens at both ends. Losses will arise from blockage of the screens and friction of the small tubes.

The screens are 18 mesh with 0.01 inch wire diameter. This gives a blockage coefficient, β = open area/total area, of $\beta = 0.52$. From experimental results of resistance coefficients for screens of different blockage coefficients [3, p. 648], we obtain $K = 1.8$ for each screen. With reference to the test section, $K_o = K(\frac{A_o}{A})^2$ where A_o = area of test section = 225 in^2 and A = area of inlet section = 4,489 in^2, we obtain $K_o = .0091$.

The loss through the soda straw section is primarily friction resistance of laminar flow through a tube. For straws of 3/16 inch diameter with a flow velocity of 12 ft/sec, the Reynolds number based on diameter is $Re_d = 1200$ which is considerably less than the critical Reynolds number for flow becoming turbulent in a tube. The laminar resistance coefficient then becomes $\lambda = 0.053$, which results in a static pressure loss coefficient of $K_o = 0.0053$.

A-2. Screens

The upstream settling chamber has four 18 mesh screens. Using the same values as we used in determining the loss coefficient for screens in the honeycomb section, we obtain $K_o = 0.0127$.

A-3. Contraction

Assuming a smooth curve, Pope [6, p. 72] gives $K_o = 0.32\ \lambda\ L/D_o$ where λ = skin friction coefficient, L = length of section, and D_o = effective diameter of the test section. The skin friction coefficient is determined as a function of Reynolds number using an empirical relation established by Prandtl for smooth pipes at high Reynolds number, $\frac{1}{\sqrt{\lambda}} = 2 \log_{10} Re \sqrt{\lambda} - 0.8$ [12, p. 515]. In our case $\lambda = 0.012$ which results in $K_o = 0.0177$.

A-4. Test Section

The losses in the test section are assumed to be greatest when running in open jet configuration. Thus the losses are calculated for a system consisting of 12 feet, 8 inches of closed duct and 10 inches of open jet using the relation for pressure loss along a pipe,

$K_o = \lambda \frac{L}{D}$ where L = length of section and D = effective diameter.

For the closed duct portion of the test section, Prandtl's universal law of friction for smooth pipes gives $\lambda = 0.0108$. The loss coefficient becomes $K_o = 0.1137$.

An estimate of friction coefficient for the open jet based on free jet considerations is $\lambda = 0.08$. For an open jet length of 10 inches, we have $K_o = 0.0513$.

A-5. Muffler-Diffuser

The duct in the first half of the muffler experiences

little divergence due to the cruciform wedge. Rough-walled pipe considerations applied to this first section yield $K_o = 0.0141$.

Diffusing action takes place in the second half. The area increase is that of a cone with vertex angle of 26°. Diffuser efficiency for this angle is $\eta_D = 0.6$ [3, p. 56]. Using the relation $K_o = (1 - \eta_o)[1 - (\frac{A_o}{A_2})^2]$ [3, p. 63], we obtain $K_o = 0.384$.

The downstream soda straw section contributes a pressure drop coefficient of $K_o = 0.0038$. This is obtained by using the Blasius formula for frictional resistance of smooth circular pipes $\lambda = 0.3164\ Re_D^{-1/4}$.

A-6. Blower Exit

The kinetic energy of the air from the blower can be considered entirely lost. Consideration of this gives $K_o = 1.0\ (\frac{A_o}{A})^2$ where A_o = test section area and A = blower discharge jet area. The fan specifications show a discharge area of 7.8 ft², but we will assume jetting reduces this area by one-fourth. The pressure drop coefficient is $K_o = 0.071$.

A-7. Sum of Static Pressure Loss Coefficients

Section	K_o	% Total Loss
Inlet screens	.0091	1.2
Honeycomb	.0053	0.7
Screens	.0127	1.9

Contraction		.0177	2.6
Closed duct		.1137	16.7
Open jet		.0513	7.5
Muffler-diffuser			
	1st half	.0141	2.1
	2nd half	.3840	56.3
Downstream honeycomb		.0038	0.6
Blower exit		.0710	10.4
	$\Sigma K_o =$	.6827	100.0

Using Pope's energy ratio, $ER = \frac{\text{jet energy}}{\Sigma \text{ circuit losses}} = \frac{1}{\Sigma K_o}$ [6, p. 69] we get:

$$ER = \frac{1}{\Sigma K_o} = \frac{1}{.6827} = 1.466.$$

Moreover, the total drop in static pressure is obtained from $\Delta p = \Sigma K_o \cdot q_o$ where q_o = dynamic pressure at the test section. Assuming a maximum velocity of 180 ft/sec at the test section, this results in a total drop of static pressure $\Delta p = 5.08$ inches of water. This loss must be balanced by the pressure rise through the fan.

B. Power Factor Measurement

The above power factor estimations indicate that a fan is required with a capacity of 16,800 cfm against a static pressure of 5 inches. The Chicago Blower centrifugal fan size 36 1/2 fills this requirement with a motor of 16 h.p. power rating.

Actual measurements of the static pressure loss in the finished wind tunnel reveal that 15.8 h.p. is required to provide a static pressure rise through the fan of 5.14 inches of water when the test section velocity is 180 ft/sec. The estimated value for this same design point was a static pressure rise of 5.08 inches through the fan which shows agreement within 1 %. However, the loss coefficient for the section upstream of the open jet is found to be K_o = 0.0318 as compared to an estimated value of K_o = 0.0862. Thus, we have less drag in the upstream sections and slightly more drag in the downstream sections than was anticipated.

IV. Tunnel Performance

A. Aerodynamic Performance

The most critical point in the final analysis of any wind tunnel is how it performs at the test section. Three important performance checks are: (1) the velocity profile across the test section, (2) the turbulence level profile across the test section, and (3) the boundary layer profile at the wall.

A-1. Open-Jet Velocity Profile

The mean velocity profile across the test section was determined using a constant temperature hot wire anemometer. The DC bridge voltage in such a unit is a direct indication of the mean velocity at the probe. The actual profile (Figure 12) of the duct 1 inch upstream from the jet edge shows a symmetrical velocity distribution. Outside the boundary layer the flow is remarkably uniform. This flat distribution was also confirmed by a number of standard pitot-static traverses. The jet edge at this point is 6 feet down the duct from the exit of the contraction section.

A check on the boundary layer thickness at this point gives an indication of the velocity profile upstream, assuming the boundary layer thickness is linear with distance. Taking the relation, $\delta(x) = 0.37 \times (\frac{ux}{\nu})^{-1/5}$ [12, p. 537], one obtains a boundary layer thickness of 1.28 inches for the flow at the test section if the boundary

layer begins at the exit of the contraction section. However, the results show a boundary layer thickness δ = 1.03 inches. Using the above equation, one can project back to find that the boundary layer begins slightly into the duct from the contraction exit. Another conclusion from this is that the velocity profile at the exit of the contraction is uniform and no large scale separation is occurring.

A-2. Open-Jet Turbulence Level Profile

The turbulence levels associated with the mean velocity profile in Figure 12 are shown in Figure 13. The turbulence level is given in percent $T\% = 100 \cdot \frac{\sqrt{\overline{u^2}}}{U}$ where u is the fluctuating longitudinal velocity component and U is the corresponding mean velocity. Again the measurements were taken with a constant temperature hot wire anemometer. Symmetry of the profile is evident. As expected the levels are greater as the walls are approached, but the level is uniform over the entire region outside the boundary layer, with a value of 0.17 % at a mean flow velocity of 32.2 m/sec. At higher velocities, the turbulence levels decrease to a minimum of 0.15 % at a flow velocity of 58 m/sec. Lower velocities result in increased turbulence levels, e.g. at a velocity of 16 m/sec the level is 0.4 %.

A-3. Boundary Layer Upstream of an Open Jet

The boundary layer profile (Figure 14) taken at a

point 1 inch upstream from the jet edge shows a boundary layer thickness of approximately 1 inch. That it is turbulent can be seen from the shape of the profile. Appropriate boundary layer parameters for this profile are:

Boundary layer thickness	δ = 1.03 inches
Displacement thickness	δ^* = 0.130 inches
Momentum thickness	θ = 0.106 inches.

Applying these parameters to the determination of the wall shear stress by the use of the relation $\tau_o/\rho_o U^2 = 0.225\ (\nu/U\delta)^{1/4}$ [12, p. 536], one obtains the friction velocity defined as $v_* = \sqrt{\tau_o/\rho_o}$. Using δ = 1.03 inches, we get v_* = 1.16 m/sec. This, in turn, is used in plotting a dimensionless velocity distribution in the boundary layer. The distribution is the "law of the wall" and "law of the wake" for turbulent boundary layers established by Coles [13]:

$$\frac{u(y)}{v_*} = \frac{1}{K} \ln \left(\frac{yv_*}{\nu}\right) + c + \frac{\pi_o}{K} \omega \left(\frac{y}{\delta}\right).$$

The constants K = 0.40, c = 5.1, and π_o = 0.55 are found to be valid for all boundary layer flows. The wake function $\omega(\frac{y}{\delta})$ can be approximated $\omega(\frac{y}{\delta}) \cong 1 + \sin \pi \left(\frac{y}{\delta} - \frac{1}{2}\right)$ [14, p. 6].

On a semi-log plot our data fits the law of the wall as evidenced by a slope of 5.75 in the intermediate region (Figure 15). This gives K = 0.41 which agrees with Coles' results. The slope intercept at $\frac{yv_*}{\nu} = 1$ gives c = 5.1. The solid line is a plot of Coles' relation.

V. Summary and Conclusions

A low-noise, low-turbulence wind tunnel has been designed according to the following aerodynamic and acoustic criteria:

(a) A uniformly distributed maximum mean velocity of 180 ft/sec through a 15 inch square open--or closed--jet test section,

(b) A turbulence level of 0.1 % in the uniform mean velocity region at the test section,

(c) A background noise level in the test chamber 10 db below signal level for each type of test contemplated,

(d) A signal level measurement low frequency cutoff of 200 cps.

Test results indicate that the specifications (a) and (b) have been met successfully. Moreover, tunnel drag losses and power requirements were estimated accurately, thus showing that Pope's method can be applied with good results.

REFERENCES

1. LIGHTHILL, M. J., "On Sound Generated Aerodynamically," Proc. Roy. Soc., Series A, Vol. 211, March 1952.

2. Private Communication with Professor Erik Mollo-Christensen, Massachusetts Institute of Technology.

3. PANKHURST, R. C. and D. W. HOLDER, Wind-Tunnel Technique, Sir Isaac Pitman and Sons Ltd., London, 1965.

4. DRYDEN, H. L. and I. H. ABBOTT, The Design of Low-Turbulence Wind Tunnels, NACA Report 940, 1949.

5. SCHUBAUER, G. B., W. G. SPANGENBERG, and P. S. KLEBANOFF, Aerodynamic Characteristics of Damping Screens, NACA TN 2001, 1950.

6. POPE, A. and J. HARPER, Low-Speed Wind Tunnel Testing, John Wiley and Sons, New York, 1966.

7. BATCHELOR, G. K. and F. S. SHAW, "A Consideration of the Design of Wind Tunnel Contractions," Australian Council for Aeronautics Report ACA-4, March 1944.

8. TSIEN, H. S., "On the Design of the Contraction Cone for a Wind Tunnel," Journal of the Aeronautical Sciences, February 1943.

9. MAESTRELLO, L., "UTIA Air Duct Facility for Investigation of Vibration Noise Induced by Turbulent Flow Past a Panel," UTIA Technical Note No. 20, April 1958.

10. BERANEK, L. L., Noise Reduction, McGraw-Hill Book Co., New York, 1960.

11. HARRIS, C. M., ed., Handbook of Noise Control, McGraw-Hill Book Co., New York, 1957.

12. SCHLICHTING, H., Boundary Layer Theory, McGraw-Hill Book Co., New York, 1960.

13. COLES, D., "The Law of the Wake in the Turbulent Boundary Layer," J. Fluid Mech., 1, Part 2, p. 191-226.

14. LEEHEY, P., "A Review of Flow Noise Research Related to the Sonar Self Noise Problem," U. S. Navy BuShips, ASW Sonar Tech. Report No. 4110366, March 1966.

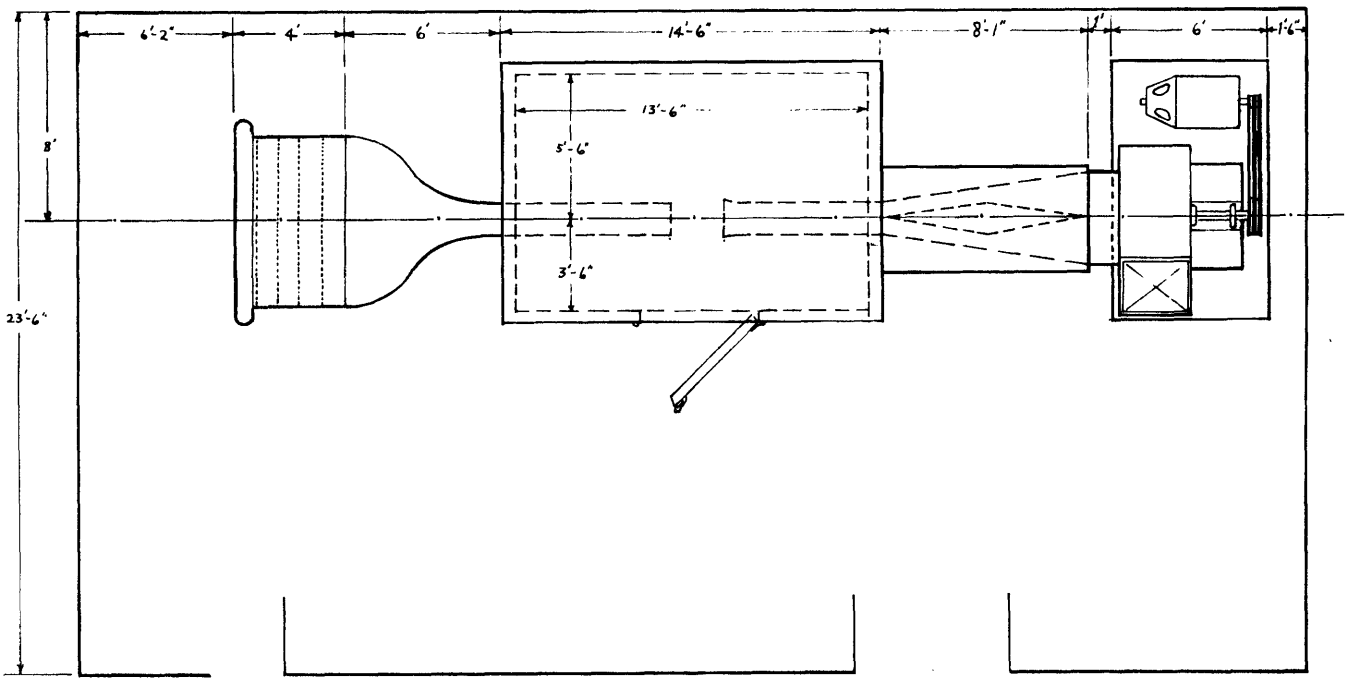

PLAN VIEW SCALE : 2'

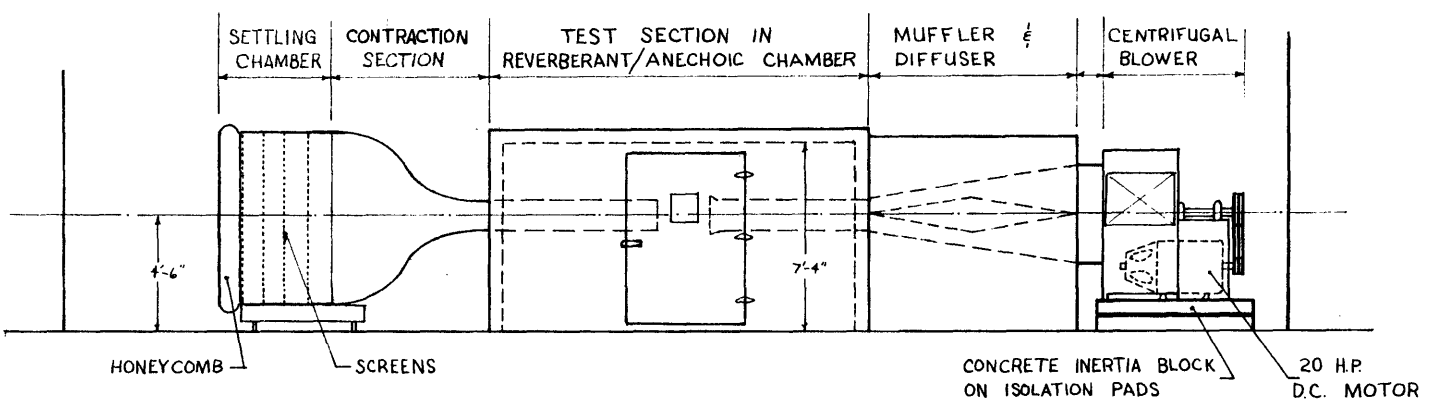

ELEVATION SCALE : 2'

GENERAL SPECIFICATIONS :
CONTRACTION RATIO : 20 : 1
TEST SECTION : 15" x 15" SQUARE , OPEN OR CLOSED

FIGURE 1. GENERAL LAYOUT.

WIND TUNNEL FACILITY - ROOM 5-024
ACOUSTICS & VIBRATIONS LABORATORY
MASSACHUSETTS INSTITUTE OF TECHNOLOGY
CEH 8-22-66

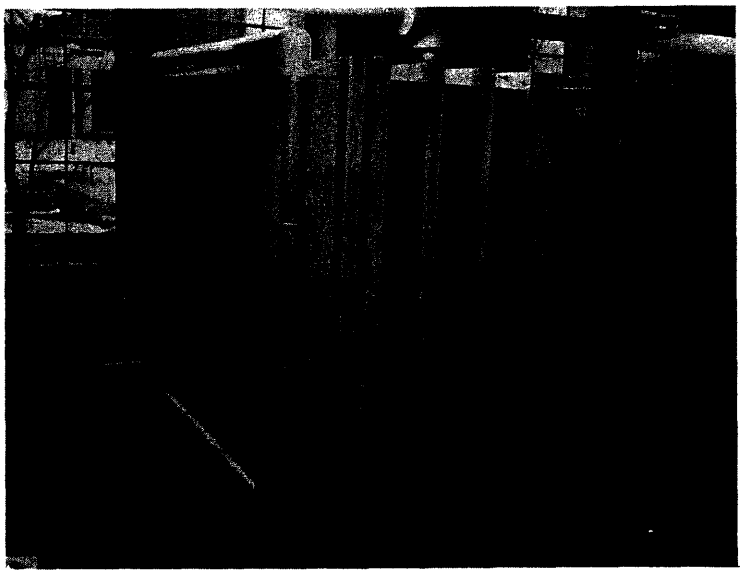

FIGURE 2. UPSTREAM SECTION INCLUDING THE INLET, HONEYCOMB, SCREENS AND CONTRACTION.

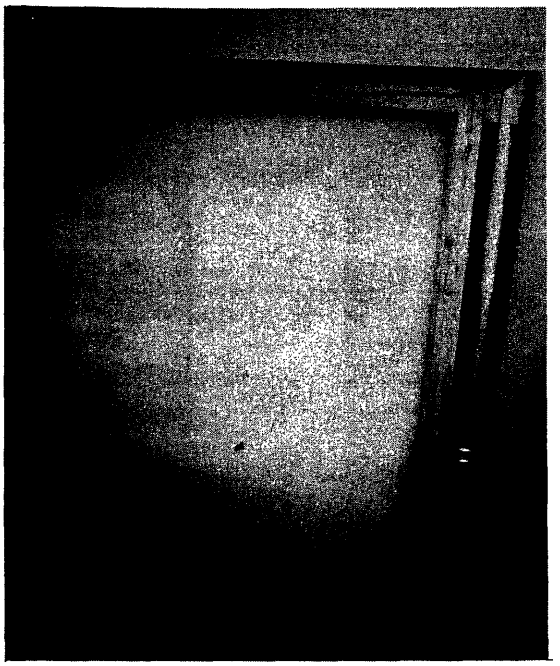

FIGURE 3. UPSTREAM HONEYCOMB OF STACKED SODA STRAWS.

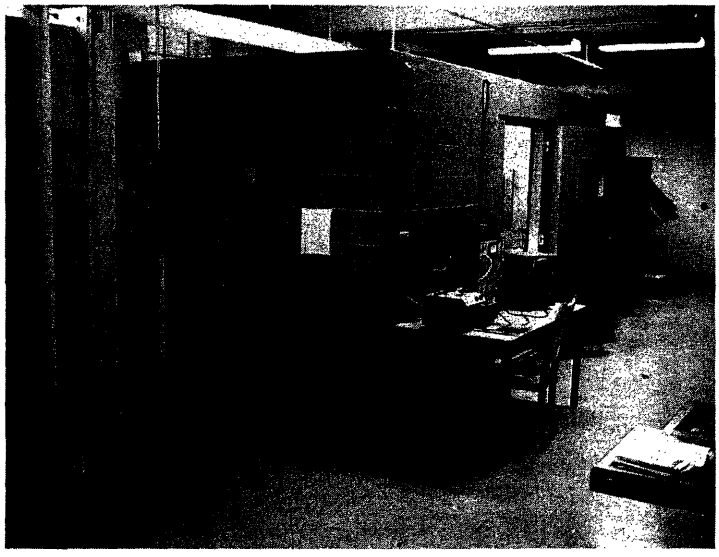

FIGURE 4. UPSTREAM PENETRATION OF REVERBERANT/ANECHOIC TEST CHAMBER.

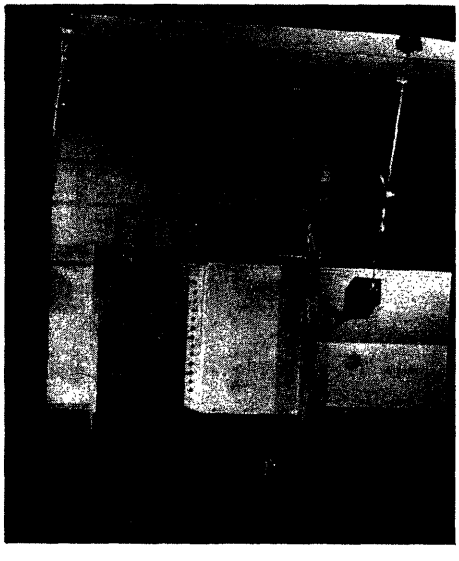

FIGURE 5. OPEN JET TEST SECTION.

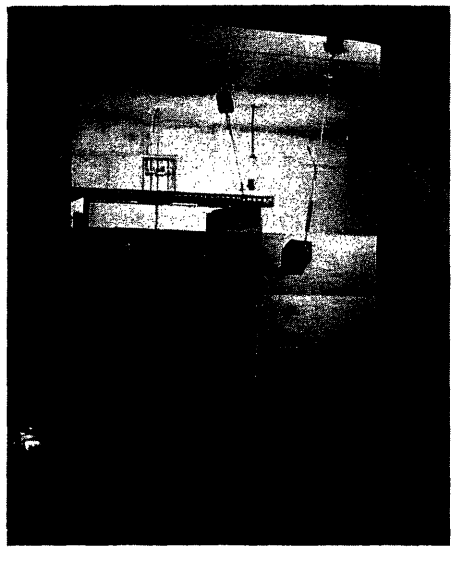

FIGURE 6. CLOSED DUCT TEST SECTION.

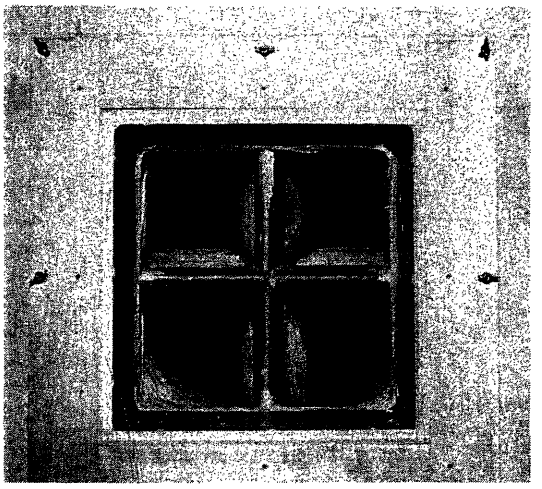

FIGURE 7. MUFFLER-DIFFUSER SECTION, LOOKING DOWNSTREAM FROM INSIDE TEST CHAMBER.

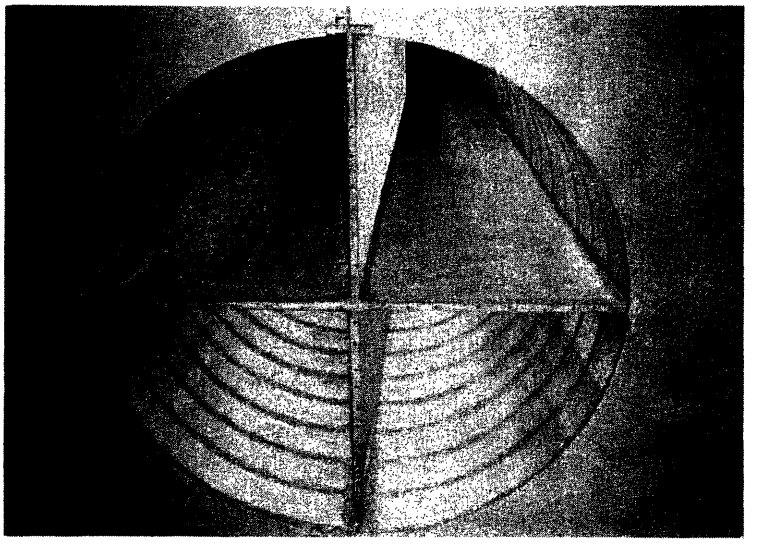

FIGURE 8. MUFFLER-DIFFUSER SECTION, LOOKING UPSTREAM FROM THE FAN.

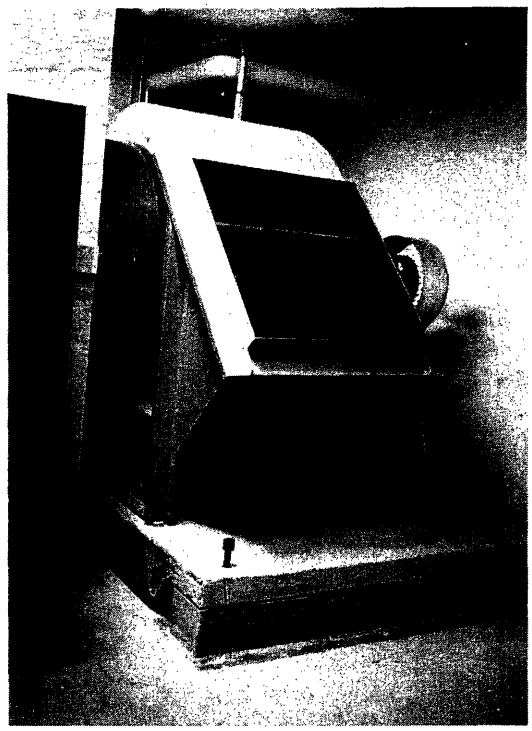

FIGURE 9. CENTRIFUGAL FAN ON VIBRATION ISOLATION BASE. THE ADJUSTABLE-GAP COUPLING IS IN FULLY CLOSED POSITION.

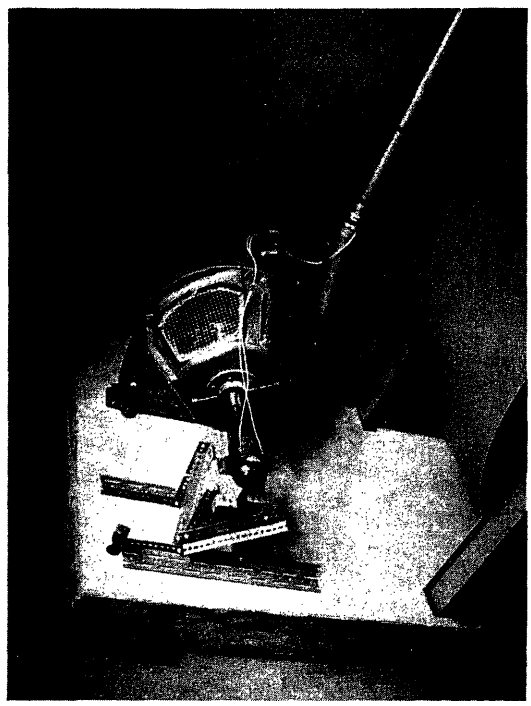

FIGURE 10. THE 20 HORSEPOWER DC MOTOR AND DRIVE UNIT.

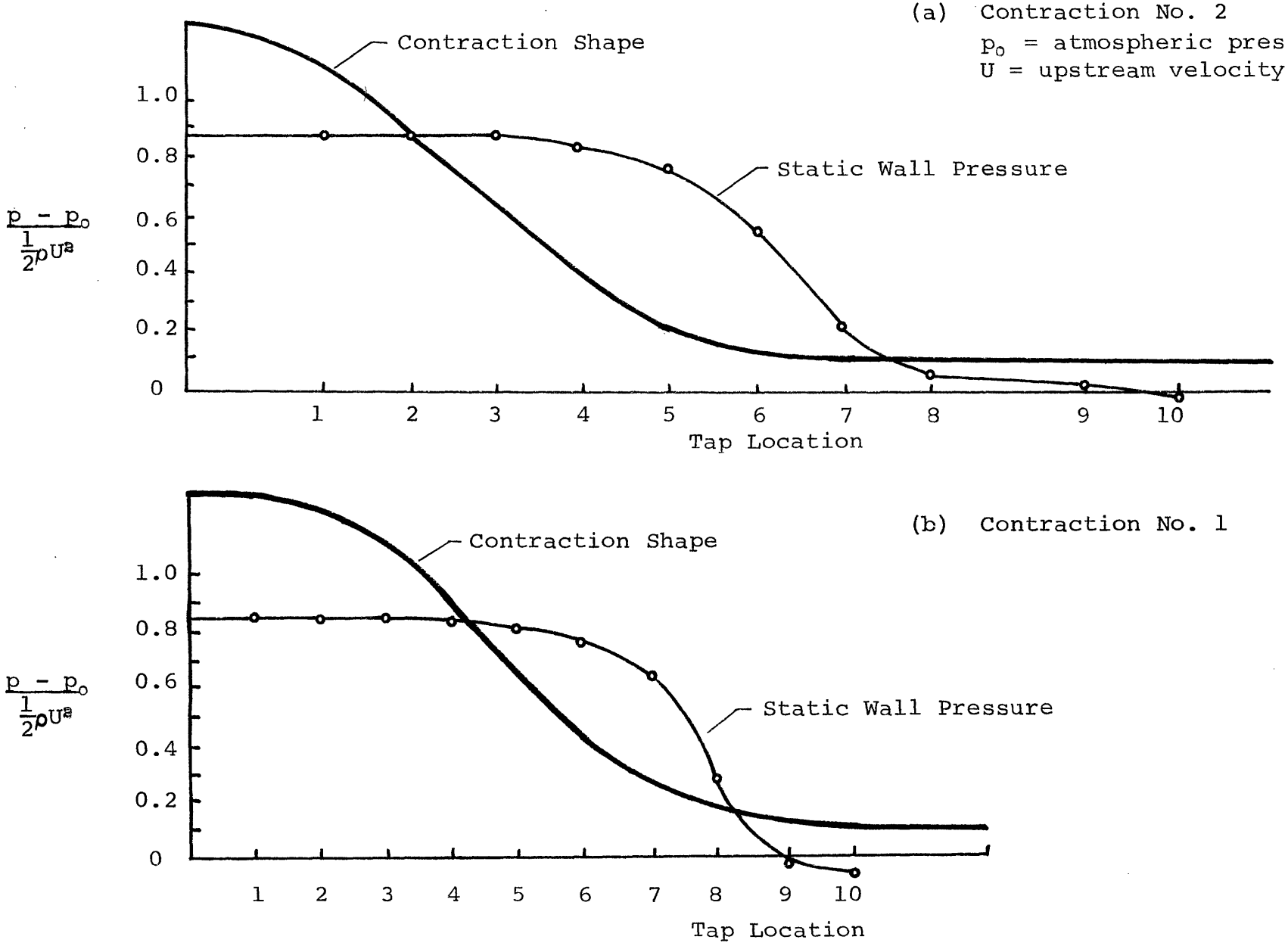

FIGURE 11. STATIC PRESSURE DISTRIBUTION ALONG MODEL CONTRACTION SECTION WALL.

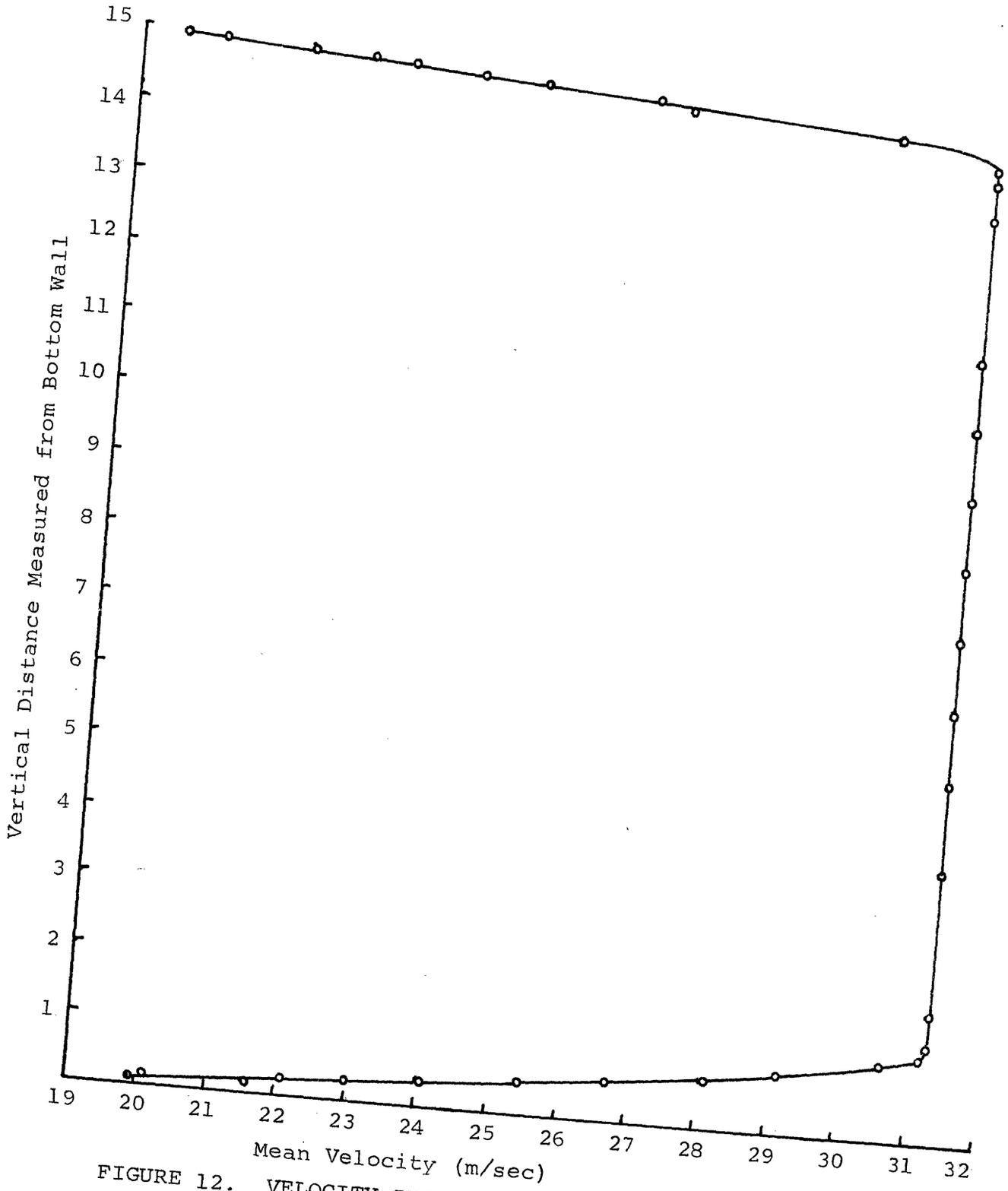

FIGURE 12. VELOCITY PROFILE IN DUCT 1 INCH UPSTREAM OF OPEN JET TEST SECTION.

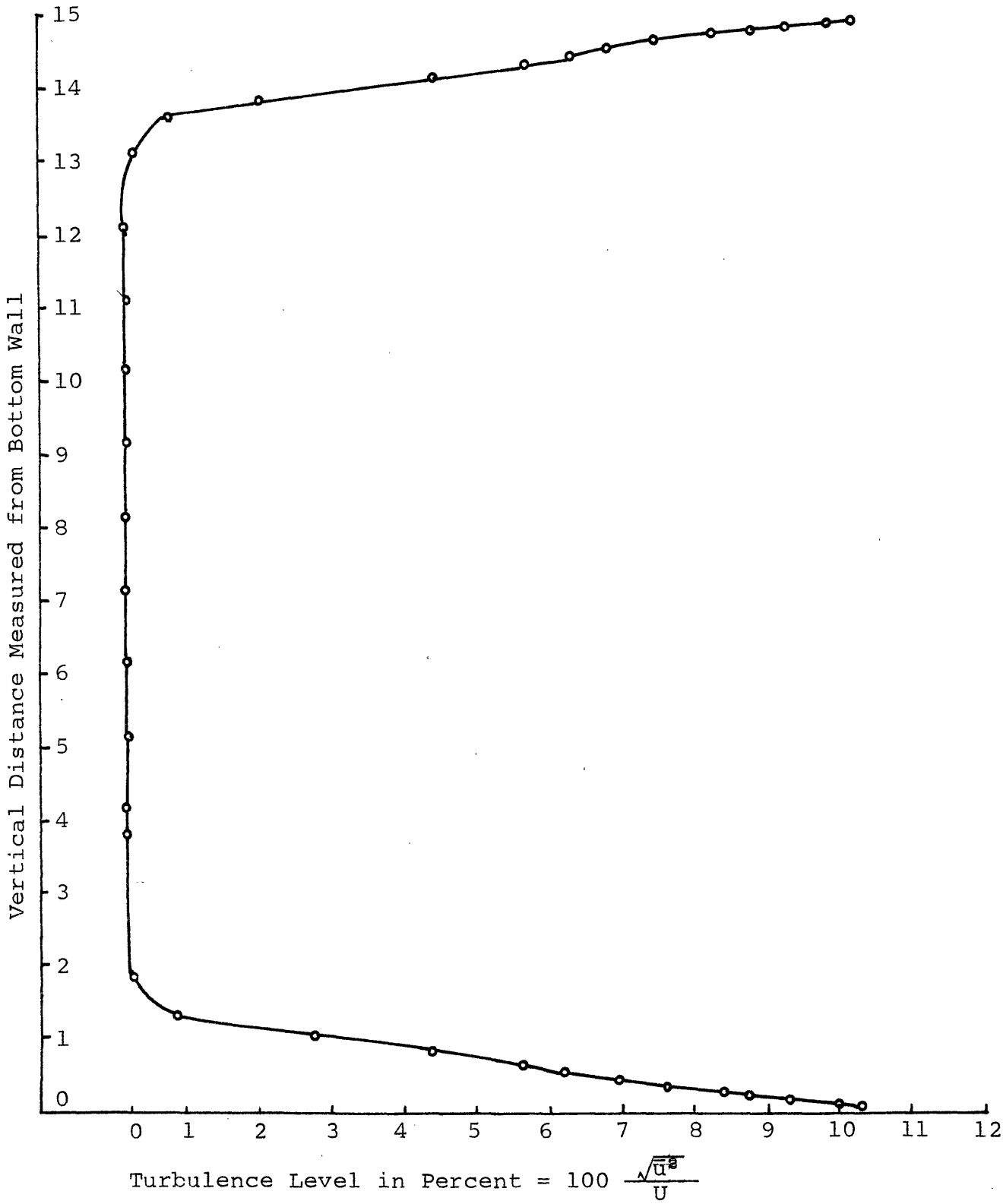

FIGURE 13. TURBULENCE PROFILE IN DUCT 1 INCH UPSTREAM OF OPEN JET TEST SECTION.

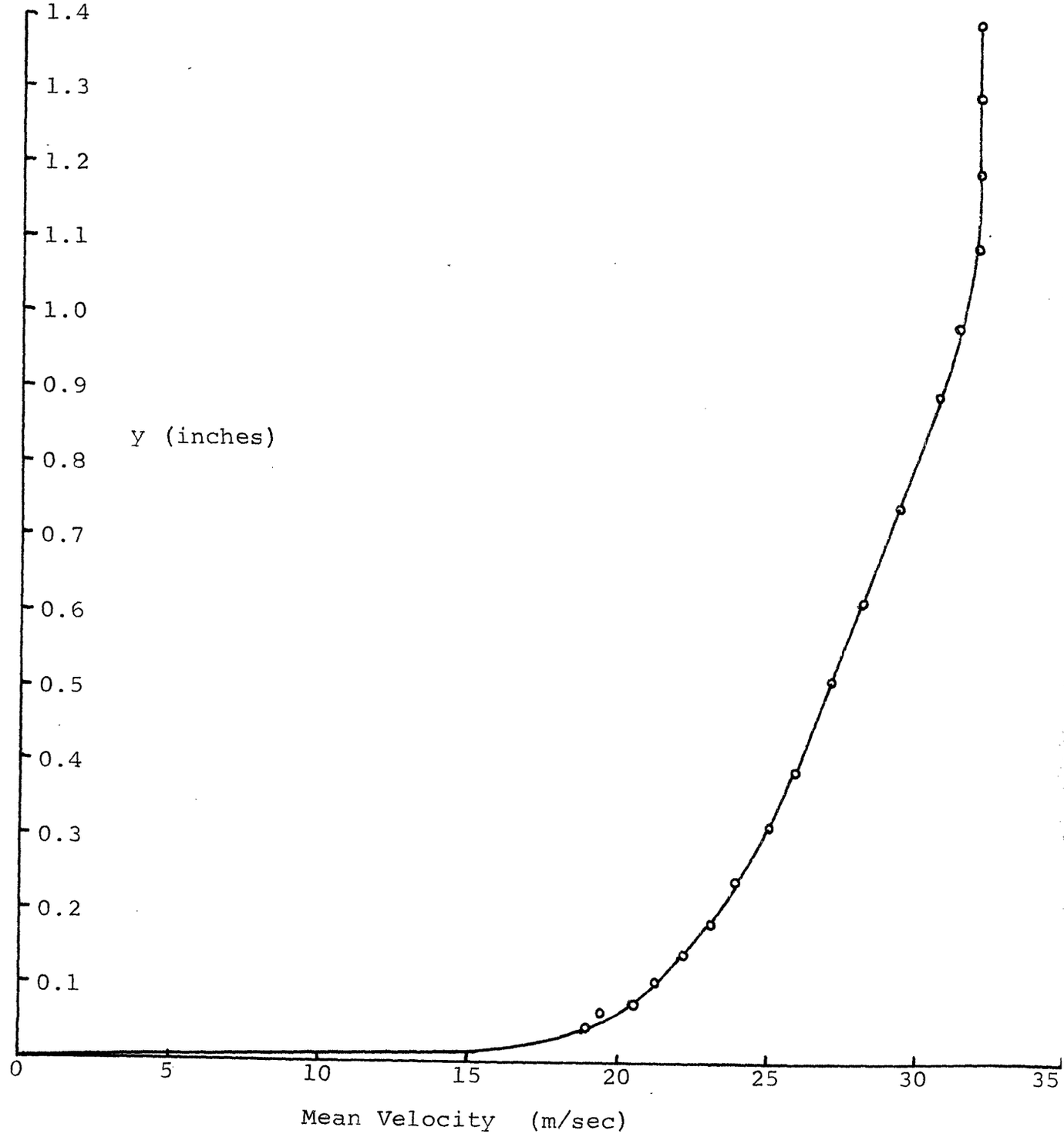

FIGURE 14. BOUNDARY LAYER MEAN VELOCITY PROFILE IN DUCT 1 INCH UPSTREAM OF OPEN JET TEST SECTION.

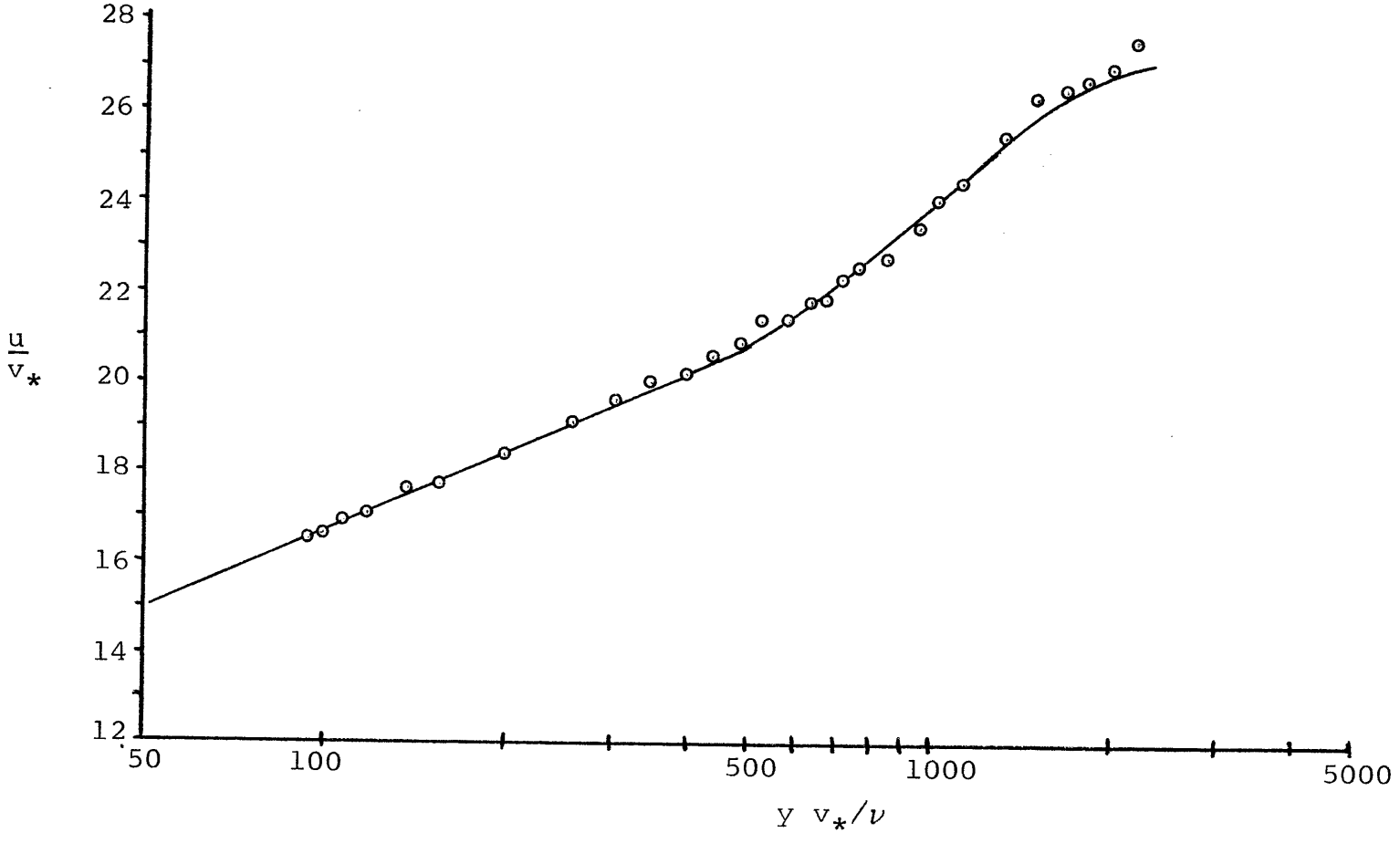

FIGURE 15. DIMENSIONLESS VELOCITY DISTRIBUTION IN THE BOUNDARY LAYER.